# High-Pressure Synthesis of Amorphous Si₃N₄ and SiBN-Based Monoliths without Sintering Additives

*Wei Li, Shuailing Ma,\* Siwen Cui, Jingxue Ding, Marc Widenmeyer, Xiaoqi Zhang, Ying Zhan,\* Zhaoju Yu, Jiarong Cheng, Pinwen Zhu, Tian Cui, Anke Weidenkaff, and Ralf Riedel*

Amorphous Si₃N₄ and SiBN monoliths without sintering additives are successfully prepared by high-pressure–low-temperature (HPLT) sintering using the single-source-precursor-derived amorphous Si₃N₄ and SiBN powders as raw materials. The microstructural evolution and crystallization behavior of the as-prepared samples are investigated using scanning electron and transmission electron microscopy and X-ray powder diffraction, respectively. The results show that the incorporation of boron in the Si–N network enhances the crystallization temperature up to 1200 °C. The Vickers' hardness of the HPLT-sintered Si₃N₄ sample amounts ≈11.6 GPa whether prepared at 1000 or 1200 °C, while the maximum hardness of the SiBN sample is up to 16.3 GPa. The fracture toughness of amorphous Si₃N₄ and SiBN5 samples is almost identical (around 2.5 MPa m$^{1/2}$) whether prepared at 1000 or 1200 °C, and SiBN2 and SiBN5 samples show an improved fracture toughness. In addition, the oxidation resistance of the as-prepared samples is investigated at temperatures up to 1000 °C. A comparison between amorphous Si₃N₄ and SiBN monoliths demonstrates a positive effect of the presence of boron on their oxidation resistance.

## 1. Introduction

Nowadays, nitride-based ceramics, such as BN, Si₃N₄, transition metal nitrides, and ternary and multinary nitrides (e.g., SiON, SiAlON, SiBCN, and so on), have shown enormous potential for applications in various industrial and energy fields.[1–4] Among these materials, polycrystalline Si₃N₄ and BN have been proved to be the most widely used nitrides due to their chemical stability, low dielectric properties, high thermal conductivity, and outstanding corrosion resistance under a broad range of temperatures. However, there is very limited study exploring the preparation and properties of amorphous Si₃N₄- and BN-based materials as compared to several kinds of polycrystalline Si₃N₄- and BN-based composites which have been extensively studied in the last two decades.[4–6]

Amorphous ceramics are considered to be the second state of matter in parallel with crystalline ceramic phases.[7] Compared to crystalline materials, amorphous materials possess much more disordered structure, highly homogeneous sites down to the atomic scale, composition flexibility, isotropic molecular diffusion, and more percolation pathways in solid mixtures, providing them unique properties in terms of electrical/thermal conductivity,[8] mechanical strength,[9] corrosion and abrasion resistance,[10] etc., and rendering them as an interesting class of structural materials.[11] In addition, bulk amorphous

W. Li, S. Ma, J. Cheng, T. Cui
School of Physical Scientific and Technology
Institute of High Pressure Physics
Ningbo University
Ningbo 315211, China
E-mail: mashuailing@nbu.edu.cn

W. Li, J. Ding, M. Widenmeyer, Y. Zhan, A. Weidenkaff, R. Riedel
Department of Materials and Earth Sciences
Technical University of Darmstadt
64287 Darmstadt, Germany
E-mail: ying.zhan@tu-darmstadt.de

The ORCID identification number(s) for the author(s) of this article can be found under https://doi.org/10.1002/adem.202400677.

S. Cui, X. Zhang, P. Zhu
Synergetic Extreme Condition High-Pressure Science Center
State Key Laboratory of Superhard Materials
College of Physics
Jilin University
Changchun 130012, China

Z. Yu
College of Materials
Ministry of Education
Key Laboratory of High Performance Ceramic Fibers (Xiamen University)
Xiamen 361005, P. R. China

A. Weidenkaff
Fraunhofer Research Institution for Materials Recycling and Resource Strategies IWKS
63755 Alzenau, Germany

**ADVANCED
SCIENCE NEWS**

www.advancedsciencenews.com

**ADVANCED
ENGINEERING
MATERIALS**

www.aem-journal.com

ceramics possess no grain boundaries if compared with polycrystalline materials influencing also abovementioned features. In the family of amorphous materials, the synthesis of bulk amorphous ceramics is challenging. In particular, amorphous covalent compounds such as $Si_3N_4$ and BN are difficult to be consolidated at low temperatures due to their low-diffusion coefficients, and at high temperatures crystallization will occur.[12,13] Therefore, to find efficient, convenient, and general methods to prepare bulk amorphous ceramics is of scientific interest.

The polymer-derived ceramic (PDC) route is an attractive method for the preparation of advanced amorphous ceramic materials and exhibits significant advantages compared to the traditional ceramic processing techniques.[14–17] The PDC route not only produces amorphous ceramics with unique phase composition and microstructures by designing the preceramic polymers, but also provides a method to prepare bulk amorphous ceramics (e.g., SiC, BN, SiCN, SiOC, SiHfN, and so on).[18–22] However, reaching fully dense bulk materials is difficult because pyrolysis of the green parts is accompanied with release of gaseous decomposition products, which negatively influences the final density of the obtained bulk ceramics. Consequently, it would be desirable to find an alternative processing technique that can combine the advantages of PDCs with that of highly dense amorphous ceramic products. Naturally, it is conceivable that lowering the sintering temperature by increasing the pressure could consolidate such covalent materials. In recent years, some fundamental works have proved that dense amorphous ceramics can be prepared under high pressure and low temperature (HPLT) and showed outstanding high-temperature properties.[23,24]

Therefore, the motivation of this work is to produce dense amorphous $Si_3N_4$ and SiBN-based monoliths by applying the HPLT technique. The influence of temperature and boron content on the attained density, phase evolution, microstructure, and mechanical properties of the amorphous products is studied and evaluated. Moreover, the oxidation resistance of the HPLT-processed amorphous $Si_3N_4$ and SiBN ceramics is also systematically characterized and discussed. This work is expected to lay the foundation for the application of the HPLT method in the preparation of a wide range of amorphous ceramics.

## 2. Experimental Section

### 2.1. Experimental Procedures

Amorphous $Si_3N_4$ and SiBN powders with a molar ratio of Si: B = 5, 2, and 1 were prepared at 1100 °C by the PDC route; the detailed single-source-precursor synthesis and pyrolysis procedures can be found in our previous work.[25] The SiBN samples with different molar ratio of Si:B = 5, 2, and 1 are denoted as SiBN5, SiBN2, and SiBN1, respectively. The as-pyrolyzed powders were dry milled in a $ZrO_2$ jar under an argon atmosphere using ball milling at 1800 rpm for 3 h and then sieved by two sieves (180 and 100 μm sieve, Merck, Darmstadt, Germany) to obtain powders less than 100 μm in size. The as-milled powder was stored in a vacuum oven at 100 °C for the subsequent HPLT experiments. The starting materials were pressed into cylinders (4 mm in diameter and 2.5 mm in height) by a hydraulic press. Hexagonal boron nitride was used as capsule to insulate the

sample with graphite heater, which prevents the chemical reaction of the sample with other carbon. The synthesis experiments were carried out on a China-type SPD 6 × 600 T cubic press, at Jilin University. The pressure of 5 GPa in the high-pressure chamber was calibrated by the phase transformation of Bi, Tl, and Ba in advance. The temperature of the sample was calibrated with a C-type thermocouple with a temperature error around 20 °C. After reaching the target pressure, the specimens were heated to the temperature of 1000–1200 °C and soaked at the target temperature for 20 min. Finally, the sample was quenched within 15 s and then cooled to room temperature. In the subsequent discussion, the prepared ceramics annealed at different temperatures are denoted as SiBN1-1000, SiBN1-1200, SiBN2-1000, SiBN2-1200, SiBN1-1000, SiBN1-1200, $Si_3N_4$-1000, and $Si_3N_4$-1200, respectively.

### 2.2. Characterization

The phase identification of the recovered samples was characterized by the X-ray diffraction (XRD) diffractometer using Cu $K\alpha_1$ radiation source (Rigaku D/Max-2500) in reflection geometry. XRD patterns of the samples oxidated at different temperatures (1000 and 1200 °C) were performed on a STADI P XRD diffractometer using Mo $K\alpha_1$ radiation source (STOE & Cie GmbH, Germany) in transmission geometry. The HPLT-sintered samples were coated with a thin layer of gold for the measurements of microstructures using a scanning electron microscope (SEM, 30 kV, JEOL JSM 7600 F, JEOL Ltd., Chiyoda, Tokyo, Japan) equipped with an energy-dispersive detector (EDS). The transmission electron microscopy (TEM) studies were conducted using a JEM-2200FS microscope (JEOL Ltd., Tokyo, Japan) coupled with an electron diffraction spectroscope (EDS, Mahwah, New Jersey, USA) and the acceleration voltage was 200 kV. The boron content of the pyrolyzed samples was analyzed at Mikroanalytisches Labor Pascher (Remagen, Germany), which was detected using inductively coupled plasma-atomic emission spectrometry. The hydrogen content of sample SiBN2 was determined at Labor Pascher by combustion in high-purity oxygen determined using infrared (IR) spectroscopy. Nitrogen and oxygen contents of the samples were measured by thermal conductivity and IR analysis, respectively. Carbon analysis was carried out by a LECO C-200 analyzer (LECO Corporation, St. Joseph, Michigan, USA) in our lab. The elemental composition of the samples pyrolyzed at 1100 °C was measured and shown in **Table 1**.

**Table 1.** Elemental composition of raw $Si_3N_4$ and SiBN materials pyrolyzed at 1100 °C.

| Samples | Composition [wt%] | | | | | | Empirical formula |
|---|---|---|---|---|---|---|---|
| | Si | B | N | H | C | O | |
| SiN | 72.14 | 0.00 | 25.83 | n.d. | 1.01 | 1.02 | $Si_{1.00}N_{0.72}(C_{0.033}O_{0.025})$ |
| SiBN5 | 69.48 | 1.67 | 25.00 | n.d. | 2.23 | 1.61 | $Si_{1.00}B_{0.06}N_{0.72}(C_{0.075}O_{0.041})$ |
| SiBN2 | 68.50 | 2.56 | 23.00 | 0.84 | 3.36 | 1.36 | $Si_{1.00}B_{0.10}N_{0.67}(C_{0.11}O_{0.04}H_{0.34})$ |
| SiBN1 | 66.73 | 4.94 | 24.41 | n.d. | 2.64 | 1.29 | $Si_{1.00}B_{0.19}N_{0.73}(C_{0.11}O_{0.034})$ |

n.d. = not determined, the error bars of Si and N content are less than ± 2.89 and error bars for other elements are less than ± 0.52.

The content of boron gradually increases, and the contents of carbon and oxygen are low, while there is about 30 wt% excess silicon in the system based on the chemical composition of $Si_3N_4$.

The HPLT-sintered specimens were polished by diamond suspension on a felt cloth for measurements of density and mechanical properties. The relative density and open porosity of the as-recovered monoliths were measured using the water immersion method (Archimedes' method). Vickers hardness measurements were performed on an HMAS-D1000SMZC microindenter with a diamond indenter under a load of 9.8 N held for 15 s. For Vickers hardness, at least five measurements were repeated to ensure the reliability of the data. The fracture toughness of the obtained samples was calculated based on reports.[26,27] The oxidation behavior of the prepared samples was investigated using thermogravimetric analysis/differential thermal analysis (TG/DTA, STA 449F3 Jupiter, Netzsch, Germany) by recording their mass change from room temperature to 1000 °C with a heating rate of 5 °C min$^{-1}$ in purified compressed air (gas purifier removes $CO_2$, $H_2O$, and hydrocarbons to ppb range, a linear gas velocity of 0.2 cm s$^{-1}$). Alumina crucibles (type DTA, 0.3 mL, Meiningen) were used for TGA/DTA measurements and the measurements were corrected for the buoyancy.

## 3. Results and Discussion

XRD patterns of the $Si_3N_4$ and SiBN samples synthesized at 1000 and 1200 °C are shown in **Figure 1**. At 1000 °C, all the recovered monoliths are predominantly X-ray amorphous. As the temperature was raised up to 1200 °C, the amorphous $Si_3N_4$ and SiBN5 specimens exhibit a low-intensity reflection of silicon, while the SiBN2 and SiBN1 samples still remain X-ray amorphous. These results demonstrate that the incorporation of boron into Si—N network has an influence on the crystallization of amorphous silicon nitride; the higher boron content suppresses the crystallization because of the higher crystallization temperature of the formed ternary Si—B—N network.[28]

The skeletal density and open porosity of the resultant specimens are presented in Figure 1b. It can be seen that the skeletal density and open porosity of amorphous silicon nitride, SiBN5, and SiBN2 samples do not change significantly with increasing temperature and boron content, which are within their error bars. However, the SiBN1 specimen exhibits clear changes compared to the other samples. This phenomenon is related to the sinterability of the amorphous starting powders prepared at 1100 °C. The samples subsequently densified under HPLT conditions at 1000 °C mainly undergo a particle arrangement and sliding process by physical force to consolidate the specimens rather than sintering as they have already seen 100 °C higher temperature during powder synthesis. The densification of boron-rich SiBN1 is difficult because the stiffness of SiBN1 particles is higher than that of amorphous $Si_3N_4$, SiBN5, and SiBN2 due to the higher boron content.[25,28] Crystallization of Si in the amorphous $Si_3N_4$, SiBN5, and SiBN2 samples, as shown by the XRD results in Figure 1a, already slowly starts to occur at 1200 °C, while the SiBN1 specimen remains X-ray amorphous at this temperature. Therefore, we have to consider that the crystallization process might hinder the densification, which will be discussed below in conjunction with SEM and TEM results.

The densification of the as-prepared amorphous $Si_3N_4$-1200 and SiBN-1200 ceramics was further studied by analyzing the polished surface, and SEM images are shown in **Figure 2**. No crystalline phase morphologies (e.g., Si and $Si_3N_4$) are detected from the SEM images, which is consistent with the XRD results. Moreover, a few isolated micropores are found in amorphous $Si_3N_4$ and SiBN5 samples, while the amorphous SiBN2 and SiBN1 specimens exhibit a dense microstructure without pores and cracks, indicating almost complete densification at 1200 °C. As reported in the literature,[25,29] a slight mass loss was detected in amorphous $Si_3N_4$ and SiBN5 ceramics by TG at ≈1200 °C. The decomposition of terminal groups $-NH_2$ and $-SiH_3$ during crystallization is the main reason for the formation of pores and cracks in amorphous $Si_3N_4$ and SiBN5 samples, which results in the release of hydrogen (Table 1) and impairs the densification of the samples.

The corresponding EDS elemental mappings of the recovered SiBN2-1200 sample are shown in Figure 2j–l. Si, B, and N are homogeneously distributed in the amorphous structure without obvious agglomeration of, e.g., binary phases such as $Si_3N_4$ and
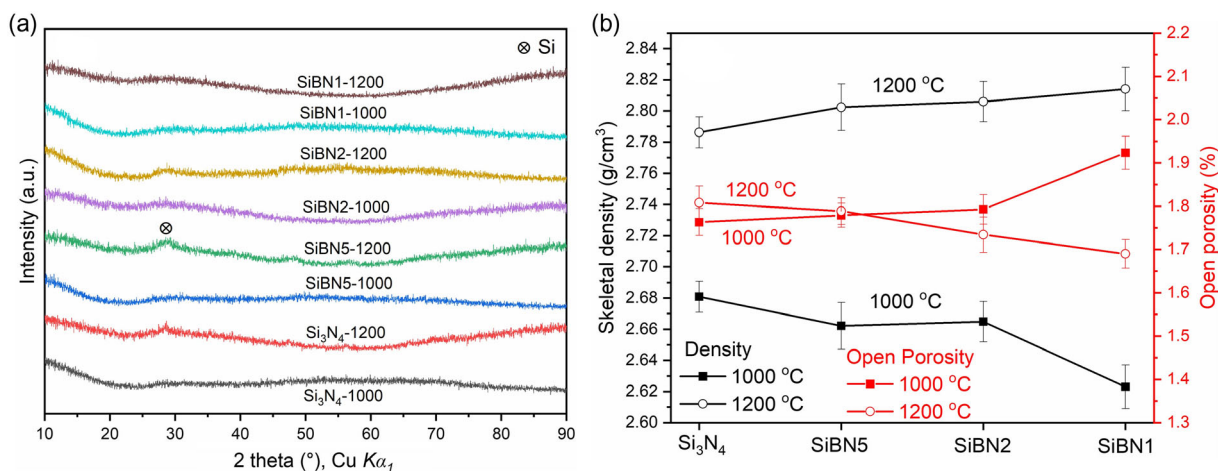


**Figure 1.** a) XRD patterns of the recovered samples synthesized under HPLT conditions at 1000 and 1200 °C. b) Skeletal density and open porosity of the HPLT-sintered samples obtained at 1000 and 1200 °C.
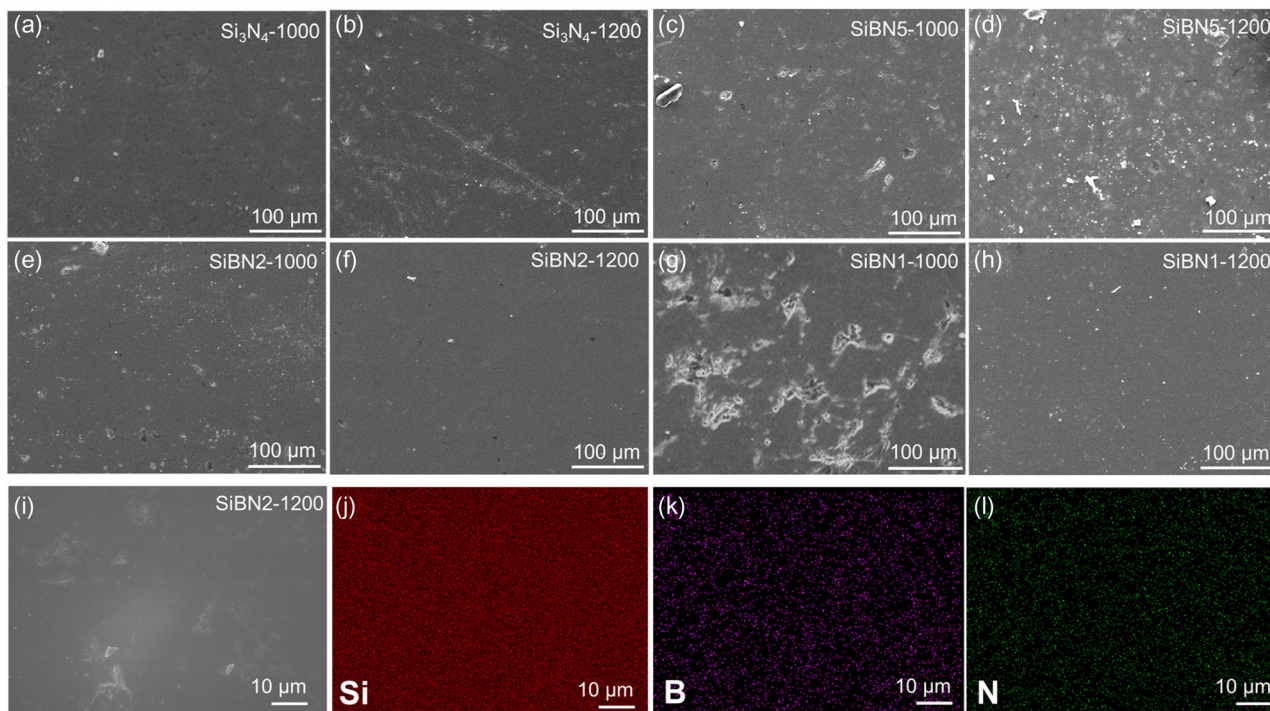
ADVANCED
SCIENCE NEWS

www.advancedsciencenews.com

ADVANCED
ENGINEERING
MATERIALS

www.aem-journal.com

**Figure 2.** SEM micrographs of the HPLT-prepared samples: a) amorphous $Si_3N_4$ at 1000 °C; b) amorphous $Si_3N_4$ at 1200 °C; c) SiBN5 at 1000 °C; d) SiBN5 at 1200 °C; e) SiBN2 at 1000 °C; f) SiBN2 at 1200 °C; g) SiBN1 at 1000 °C; h) SiBN1 at 1200 °C; i–l) SEM graph and elemental mappings of the SiBN2-1200, indicating a dense SiBN ceramic structure with homogeneous Si, B, and N elemental distribution.

BN. Molecular dynamic simulations have proven that the self-diffusion coefficient of nitrogen decreases significantly with increasing boron content in the SiBN system, while it has minor influence on the Si diffusivity, which leads to a uniform but unequal distribution of boron at the nanoscale.[30,31]

The microstructures of the HPLT-sintered amorphous $Si_3N_4$ and SiBN ceramics obtained at 1200 °C were further investigated by TEM along with the selected area electron diffraction (SAED) pattern. As shown in **Figure 3**a, the high-resolution TEM (HRTEM) image of the as-prepared $Si_3N_4$ ceramic exhibits a small amount of nanoprecipitations embedded within an amorphous matrix, which corresponds to the Si (202) lattice plane with a lattice spacing of 0.19 nm. This observation indicates that crystallization of the HPLT-sintered $Si_3N_4$ takes place at 1200 °C starting from silicon-containing regions, which is in agreement with the XRD results displayed in Figure 1. The HRTEM image and SAED pattern exhibit noticeable changes with the incorporation of boron into the amorphous Si—N network. The lattice fringes of the poorly crystallized nanoparticles in SiBN5 sample can be found in the HRTEM image (Figure 3b). Furthermore, the appearance of diffraction rings instead of spots in the SAED pattern also indicates partial crystallization of the SiBN5 sample, which is not visible from the XRD pattern shown in Figure 1. However, the HRTEM image and SAED pattern of the SiBN2 (Figure 3c) and SiBN1 (Figure 3d) sample are featureless corresponding to an amorphous nature, which is in accordance with the XRD pattern of the HPLT-prepared SiBN2 and SiBN1 sample, indicating that crystallization takes place at 1200 °C starting from boron-free regions.

The Vickers hardness of the as-prepared amorphous $Si_3N_4$ and SiBN ceramics at 1000 and 1200 °C was measured and calculated as shown in **Figure 4**. The Vickers hardness of amorphous $Si_3N_4$ ceramic is relatively stable with the change of densification temperature, whereas temperatures have a significant influence on the Vickers hardness of that of the SiBN samples. The Vickers hardness of the SiBN5-1000 and SiBN2-1000 is higher than that of the samples prepared at 1200 °C. Conversely, the changing trend of the Vickers hardness of the SiBN1-1000 and SiBN1-1200 sample is opposite. The hardness of the SiBN1 sample prepared at 1000 °C amounts 12.03 GPa, while the hardness of the 1200 °C-obtained SiBN1 sample reaches a value up to 16.32 GPa. As demonstrated by XRD and TEM, the crystallization of SiBN5 and SiBN2 at 1200 °C leads to the formation of Si (low hardness ≈11 GPa)[32] and a small amount of pores, thus resulting in the hardness of SiBN5-1000 and SiBN2-1000 being higher than the specimens sintered at 1200 °C. SiBN1-1200 still remains amorphous, as a consequence, it not only occurs particle arrangement and sliding but also densification without crystallization, leading to a significant increase in the Vickers hardness. This finding is in line with the analyzed density of the samples as shown in Figure 1b. In addition, it can be seen that the Vickers hardness of the SiBN ceramics is higher than that of the amorphous $Si_3N_4$ ceramic (≈11.57 ± 0.38 GPa) except for the SiBN5-1200 sample (11.25 ± 0.61 GPa). In fact, the value is within the margin of error. Therefore, we can conclude that the addition of boron into the amorphous Si—N network is beneficial to improve hardness, which is attributed to the formation of the rigid ternary Si—B—N network. Numerous experimental and
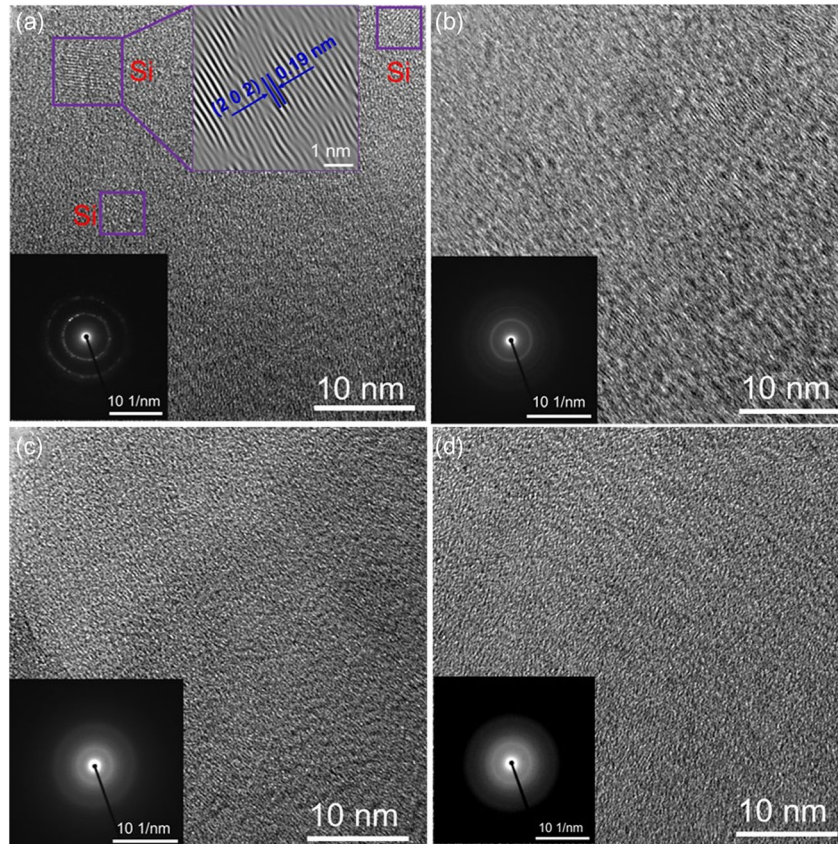
**ADVANCED
SCIENCE NEWS**

www.advancedsciencenews.com

*ADVANCED
ENGINEERING
MATERIALS*

www.aem-journal.com

**Figure 3.** High-resolution TEM images of the HPLT-prepared a) amorphous $Si_3N_4$, b) SiBN5, c) SiBN2, and d) SiBN1 samples at 1200 °C; the below insets in (a)–(d) are the SAED images; the up inset is the fast fourier transformation (FFT) image from the selected area.
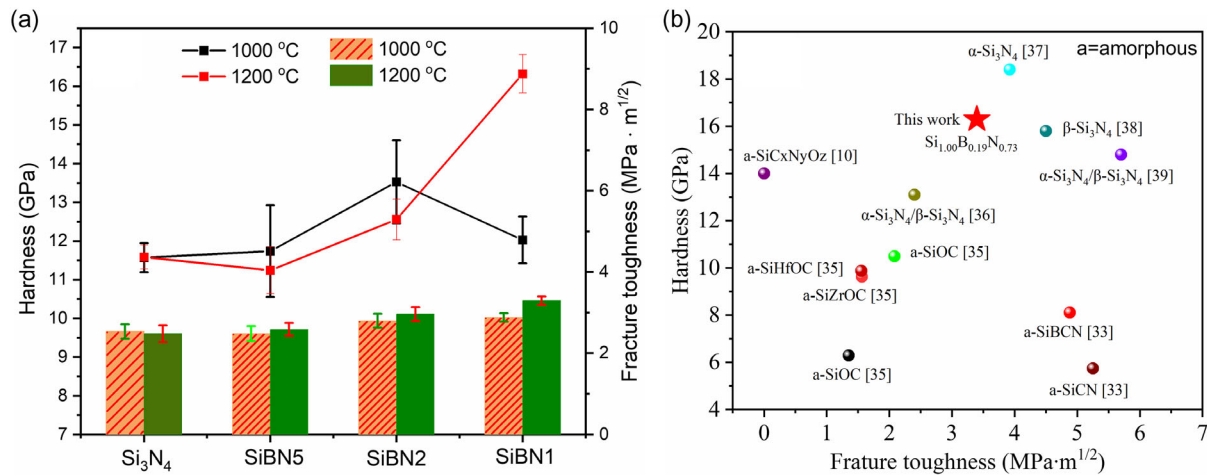


**Figure 4.** a) Vickers hardness and fracture toughness of the HPLT-sintered amorphous $Si_3N_4$ and SiBN ceramics. b) Vickers hardness and fracture toughness of SiBN1 sample (load: 9.8 N) in comparison with those of the reported amorphous/crystalline Si-based materials.

theoretical studies have proven that the atomic diffusivity of nitrogen and silicon atoms decreases with increasing boron content in Si—N networks, leading to the formation of Si—B—N networks.[25,30,31,33] Furthermore, the amorphous SiBN phase will be separated into SiN regions with less boron content, thus resulting in low hardness.

The fracture toughness of the obtained specimens was calculated based on references and shown in Figure 4a.[26,27] The fracture toughness of amorphous $Si_3N_4$ and SiBN5 samples is almost identical (around 2.5 MPa m$^{1/2}$) whether prepared at 1000 or 1200 °C, while SiBN2 and SiBN5 samples show an increased fracture toughness at the same condition.

Therefore, changes in fracture toughness are considered to relate to the presence of boron. As mentioned above, Si—B—N bonds are rigid networks, while relatively weak Si—N boundaries in SiBN matrix may act as a lubricant to improve grain boundary sliding, thereby leading to enhanced fracture toughness in SiBN specimens.[26,34] In order to comprehensively assess the hardness and fracture toughness of the obtained ceramics, a comparison with reported amorphous/crystalline Si-based materials is summarized and shown in Figure 4b. Amorphous SiBN1 samples have lower fracture toughness than crystalline β-$Si_3N_4$ or α/β-$Si_3N_4$ ceramics, but higher hardness and fracture toughness than most of the reported amorphous Si-based materials (e.g., SiHfOC, SiZrOC, SiOC, SiCN, and SiBCN).[10,33,35–39] Therefore, the high-pressure-derived amorphous SiBN1 ceramic monoliths are considered to be potential candidate materials for structural applications.

The oxidation resistance of the obtained samples was evaluated by TG at 1000 °C in air for 10 h, as shown in **Figure 5**. To the best of our knowledge, there are no reports on the oxidation properties of bulk amorphous silicon nitride. The obtained amorphous $Si_3N_4$-1000 sample shows a mass loss of 7.58 wt%; Ma et al.[40] reported that amorphous silicon nitride contains a large number of unsaturated Si—N and Si dangling bonds, which provide active sites for oxidation, leading to severe mass change. In addition, excess silicon (≈30 wt%) and <1 wt% of hydrogen also existed in the system;[25,41] therefore, the surface with $O_3$Si—H and Si—OH species could lead to the formation of suboxides (e.g., SiO) and prevent the growth of a dense $SiO_2$ layer, resulting in the continuous mass loss.[42–44] The total mass variation of the obtained monoliths is smaller than that of reported powder samples, indicating the improved oxidation of the obtained bulk amorphous silicon nitride. For example, Wen et al. demonstrated that the amorphous silicon nitride powder showed a weight loss of ≈6.5 wt% at the beginning of the heating process, which was ascribed to the decomposition of the impurities.[45] The final mass change was around 13 wt%, whereas the mass change of amorphous silicon nitride nanoparticles was as high as 25 wt% in the work of Ma et al.[40]
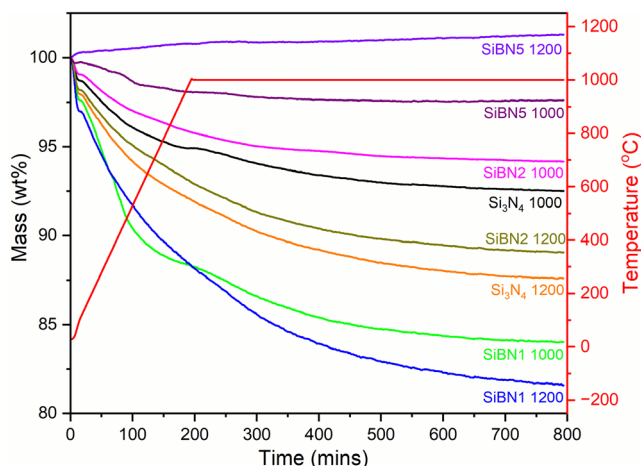
The mass changes of the SiBN5-1000 and SiBN5-1200 sample amount −1.25 wt% and 2.36 wt%, respectively, which are much smaller compared to that of the other samples. The SiBN2 samples exhibit improved oxidation resistance with respect to that of the $Si_3N_4$ samples under the same conditions, while the SiBN1-1200 sample has a negative mass change of up to 18.4 wt%, indicating that the boron content has a significant effect on the oxidation resistance of the HPLT-prepared samples. The incorporation of B into amorphous Si—N networks not only leads to the formation of rigid B—N and Si—B—N linkages, but also occupies part of the unsaturated spaces, thereby resulting in improved oxidation resistance compared to amorphous silicon nitride. However, the oxidation resistance of SiBN samples deteriorates with increasing boron content, indicating that the analyzed increased mass change correlates with increasing boron content. It is well documented in literatures that the melting point of the formed $B_2O_3$ is ≈450 °C and it starts to evaporate at ≈900 °C.[46,47] Therefore, $B_2O_3$ evaporation is likely to occur and is likely to be responsible for the severe mass loss of the SiBN1 specimen under the oxidation condition.

In order to investigate the stability of amorphous samples in air, the oxidation products of the oxidized specimens were analyzed by XRD, and the XRD patterns are presented in **Figure 6**. The broad reflections of all oxidized SiBN samples imply a low degree of crystallinity or (nearly) amorphous structure, indicating that the amorphous boron containing SiBN material possesses an enhanced crystallization resistance even at 1200 °C in air and still remains X-ray amorphous. However, boron-free $Si_3N_4$ prepared at 1200 °C crystallizes into α-$Si_3N_4$, Si, and a small amount of $Si_2N_2O$.

The cross section of the oxidated SiBN5-1000 and $Si_3N_4$-1000 samples was characterized by SEM/EDS. As can be seen in **Figure 7**, the SEM images of the SiBN5-1000 sample show an obvious oxide scale at the surface, while no obvious oxide layer was observed in the amorphous silicon nitride monolith. Furthermore, the oxide scale thickness of the obtained sample can be determined by EDS mapping, especially the distribution of oxygen element, which is between 10 and 15 μm in the
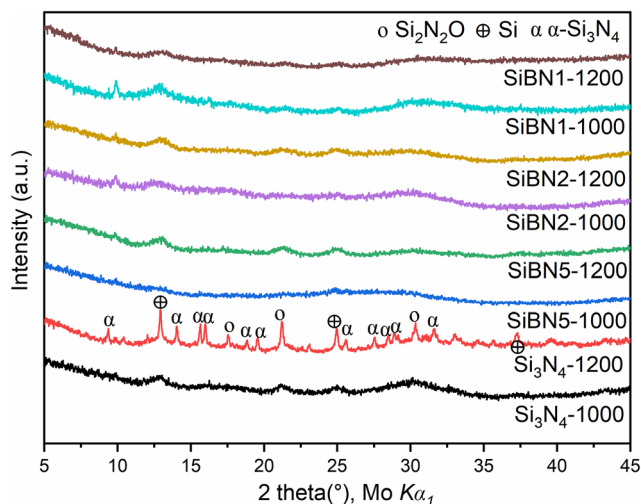
**Figure 5.** TG curves of the HPLT-prepared samples recorded at the temperature range from RT to 1000 °C and subsequent isothermal hold in air for 10 h.

**Figure 6.** XRD patterns of the HPLT-sintered samples oxidized at 1000 °C in air for 10 h.

**ADVANCED
SCIENCE NEWS**

www.advancedsciencenews.com

**ADVANCED
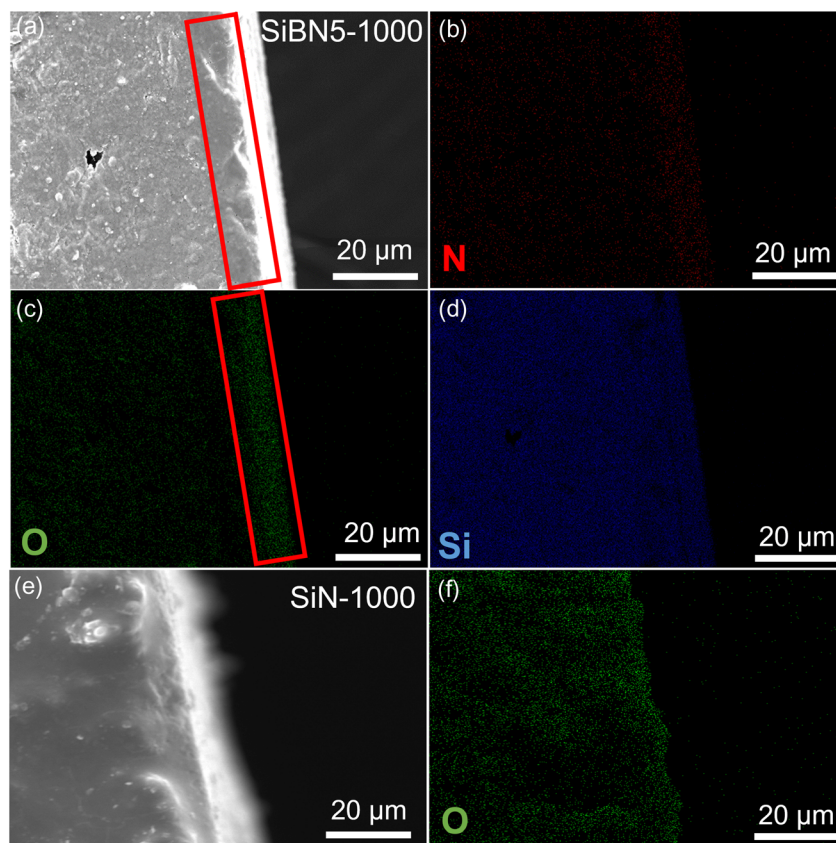ENGINEERING
MATERIALS**

www.aem-journal.com

**Figure 7.** SEM images and EDS mapping of the cross section of SiBN5-1000 (a–d) and $Si_3N_4$-1000 (e,f) sample exposed at 1000 °C under air condition.

SiBN5-1000 sample and is much lower than that of the $Si_3N_4$-1000 sample, indicating the improved oxidation resistance with the incorporation of boron in the Si—N network. Furthermore, the surface of the $Si_3N_4$-1000 sample after oxidation is rougher under the same polishing conditions, which may be related to the volatilization of small species during oxidation.

Many reports stated that the influence of boron on the oxidation resistance relies on the boron content. For example, the oxidation behavior of SiBN samples with a boron content of 0.23 wt%, 3.56 wt%, 5.14 wt%, and 6.81 wt% was investigated by Long et al.[48] the results show that the SiBN samples with boron content over 5.14 wt% were easier to be oxidized, and the escape of boron in the form of $B_2O_3$ gas at high temperatures (>1000 °C) was confirmed by X-ray photoelectron spectroscopy.[48] It is well documented in literatures that the melting point of the formed $B_2O_3$ is ≈450 °C and it starts to evaporate at ≈900 °C. Combining our work with the work reported above, it can be concluded that when the boron content is between 0.23 wt% and 1.67 wt%, it is beneficial to improve the anti-oxidation performance of the amorphous SiBN system.

## 4. Conclusion

In the present work, amorphous $Si_3N_4$ and SiBN ceramic monoliths have been successfully synthesized by HPLT sintering starting from corresponding amorphous powders synthesized

via the PDC route. The density of the samples prepared at 1000 °C decreases from 2.68 to 2.62 g cm$^{-3}$ with increasing boron content, while the density of the samples prepared at 1200 °C shows the opposite trend, increasing from 2.77 to 2.81 g cm$^{-3}$ due to partial crystallization. Therefore, high pressure provides a low-temperature way to prepare dense amorphous covalent compounds that are difficult to consolidate by conventional sintering methods. In addition, the microstructural evolution of the HPLT-sintered ceramics reveals that the crystallization of the obtained samples begins at 1200 °C starting from Si-containing regions, which has a significant influence on the hardness of the as-prepared samples. The Vickers hardness of SiBN5 (11.74 GPa) and SiBN2 (13.53 GPa) ceramic monoliths prepared at 1000 °C is higher than that of the samples SiBN5 (11.25 GPa) and SiBN2 (11.25 GPa) synthesized at 1200 °C due to beginning of crystallization. Moreover, the maximum hardness up to 16.3 GPa is achieved with the SiBN1 sample prepared at 1200 °C because of enhanced densification without crystallization. The presence of high amounts of boron obviously 1) hinders crystallization and 2) enhances densification under the HPLT conditions used in this study. Besides, amorphous SiBN5 monoliths exhibit better oxidation resistance as compared to boron-free $Si_3N_4$ due to the formation of rigid B—N and Si—B—N linkages reducing the number of unsaturated Si—N and Si dangling bonds. However, higher amount of boron as it is the case for SiBN1

reduces the oxidation resistance caused by the formation of volatile boron oxide.

The influence of low-pressure–high-temperature conditions (5 GPa and temperatures from 1400 to 1800 °C) on the phase evolution, mechanical and oxidation resistance of $Si_3N_4$ and SiBN ceramics as well as their high-temperature self-healing capability, thermal and electrical conductivities are in progress and will be reported in future studies.

## Acknowledgements

## Conflict of Interest

The authors declare no conflict of interest.

## Data Availability Statement

The data that support the findings of this study are available from the corresponding author upon reasonable request.

## Keywords

[1] W. O. Soboyejo, J. D. Obayemi, E. Annan, E. K. Ampaw, L. Daniels, N. Rahbar, *Adv. Mater. Res.* **2016**, *1132*, 385.

[2] P. Colombo, G. Mera, R. Riedel, G. D. Sorarù, *J. Am. Ceram. Soc.* **2010**, *93*, 1805.

[3] J. Eichler, C. Lesniak, *J. Eur. Ceram. Soc.* **2008**, *28*, 1105.

[4] L. Toth, in *Transition Metal Carbides and Nitrides*, Elsevier, New York, London **2014**.

[5] F. L. Riley, *J. Am. Ceram. Soc.* **2000**, *83*, 245.

[6] M. H. Bocanegra-Bernal, B. Matovic, *Mater. Sci. Eng. A* **2010**, *527*, 1314.

[7] J. C. Dyre, *Rev. Mod. Phys.* **2006**, *78*, 953.

[8] M. A. Mazo, A. Tamayo, A. C. Caballero, J. Rubio, *J. Eur. Ceram. Soc.* **2017**, *37*, 2011.

[9] S. R. Shah, R. Raj, *Acta Mater.* **2002**, *50*, 4093.

[10] T. Cross, R. Raj, S. V. Prasad, T. E. Buchheit, D. R. Tallant, *J. Am. Ceram. Soc.* **2006**, *89*, 3706.

[11] S. Jothi, S. Ravindran, L. Neelakantan, R. Kumar, *Ceram. Int.* **2015**, *41*, 10659.

[12] P. Pandi, R. Bulusu, N. Kommineni, W. Khan, M. Singh, *Int. J. Pharm.* **2020**, *586*, 119560.

[13] M. Ippolito, S. Meloni, *Phys. Rev. B* **2011**, *83*, 165209.

[14] S. T. Schwab, R. C. Graef, C. R. Blanchard, S. F. Dec, G. G. Maciel, *Ceram. Int.* **1998**, *24*, 411.

[15] B. J. Ackley, K. L. Martin, T. S. Key, C. M. Clarkson, J. J. Bowen, N. D. Posey, J. F. Ponder, Z. D. Apostolov, M. K. Cinibulk, T. L. Pruyn, M. B. Dickerson, *Chem. Rev.* **2023**, *123*, 4188.

[16] A. Viard, D. Fonblanc, D. Lopez-Ferber, M. Schmidt, A. Lale, C. Durif, M. Balestrat, F. Rossignol, M. Weinmann, R. Riedel, S. Bernard, *Adv. Eng. Mater.* **2018**, *20*, 1800360.

[17] N. Thor, G. Winkens, J. Bernauer, N.-C. Petry, K. Beck, J. Wang, R. Schwaiger, R. Riedel, U. Kolb, M. Lepple, A. Pundt, *Adv. Eng. Mater.* **2024**, 2301841.

[18] W. Li, F. Li, Z. Yu, Q. Wen, B. Fan, Y. Feng, C. Zhao, E. Ricohermoso, M. Widenmeyer, A. Weidenkaff, R. Riedel, *J. Eur. Ceram. Soc.* **2022**, *42*, 4493.

[19] W. Li, H. Du, C. Tian, T. Jiang, J. Bernauer, M. Widenmeyer, L. Wiehl, L. Molina-Luna, J. P. Hofmann, A. Weidenkaff, Z. Yu, R. Riedel, *Z. Anorg. Allg. Chem.* **2022**, *648*, e202200203.

[20] L. Bharadwaj, Y. Fan, L. Zhang, D. Jiang, L. An, *J. Am. Ceram. Soc.* **2004**, *87*, 483.

[21] S. Martínez-Crespiera, E. Ionescu, H.-J. Kleebe, R. Riedel, *J. Eur. Ceram. Soc.* **2011**, *31*, 913.

[22] H. Chen, X. Chen, J. S.-K. Lim, Y. Lu, J. Hu, Y.-N. Liang, X. M. Hu, *Adv. Eng. Mater.* **2022**, *24*, 2200269.

[23] B. Liang, Z.-H. Yang, D.-C. Jia, J.-C. Rao, D.-L. Yu, Y.-J. Tian, Q. Li, Y. Miao, Q.-S. Zhu, Y. Zhou, *Corros. Sci.* **2016**, *109*, 162.

[24] B. Liang, D. Jia, Y. Miao, Q. Zhu, X. Liao, Z. Yang, Y. Zhou, *Corros. Sci.* **2017**, *122*, 100.

[25] Y. Zhan, W. Li, T. Jiang, C. Fasel, E. Ricohermoso, J. Bernauer, Z. Yu, Z. Wu, F. Müller-Plathe, L. Molina-Luna, R. Grottenmüller, R. Riedel, *J. Adv. Ceram.* **2022**, *11*, 1104.

[26] W. Li, Z. Yu, L. Wiehl, T. Jiang, Y. Zhan, E. Ricohermoso, M. Etter, E. Ionescu, Q. Wen, C. Lathe, R. Farla, D. T. Teja, S. Bruns, M. Widenmeyer, A. Weidenkaff, L. Molina-Luna, R. Riedel, S. Bhat, *J. Adv. Ceram.* **2023**, *12*, 1418.

[27] Y. Shadangi, V. Shivam, K. Chattopadhyay, N. K. Mukhopadhyay, *J. Manuf. Mater. Process.* **2022**, *6*, 60.

[28] X. Long, C. Shao, Y. Wang, *J. Am. Ceram. Soc.* **2020**, *103*, 4436.

[29] F. L. Ma, H. M. Qi, Y. P. Zhu, X. W. Ren, F. Wang, *Key Eng. Mater.* **2013**, *575–576*, 81.

[30] K. Matsunaga, Y. Iwamoto, *J. Am. Ceram. Soc.* **2001**, *84*, 2213.

[31] N. Liao, W. Xue, M. Zhang, *Model. Simul. Mater. Sci. Eng.* **2012**, *20*, 035009.

[32] L. J. Vandeperre, F. Giuliani, S. J. Lloyd, W. J. Clegg, *Acta Mater.* **2007**, *55*, 6307.

[33] D. Li, Z. Yang, D. Jia, X. Duan, Y. Zhou, D. Yu, Y. Tian, Z. Wang, Y. Liu, *J. Eur. Ceram. Soc.* **2018**, *38*, 1179.

[34] K. Madhav Reddy, J. J. Guo, Y. Shinoda, T. Fujita, A. Hirata, J. P. Singh, J. W. McCauley, M. W. Chen, *Nat. Commun.* **2012**, *3*, 1052.

[35] T. To, C. Stabler, E. Ionescu, R. Riedel, F. Célarié, T. Rouxel, *J. Am. Ceram. Soc.* **2020**, *103*, 491.

[36] A. De Pablos, M. I. Osendi, P. Miranzo, *Ceram. Int.* **2003**, *29*, 757.

[37] M. Kitayama, K. Hirao, M. Toriyama, S. Kanzaki, *J. Ceram. Soc. Jpn.* **2000**, *108*, 646.

[38] C.-H. Lee, H.-H. Lu, C.-A. Wang, W.-T. Lo, P. K. Nayak, J.-L. Huang, *Ceram. Int.* **2011**, *37*, 641.

[39] H. Miyazaki, H. Hyuga, Y.-I. Yoshizawa, K. Hirao, T. Ohji, *J. Eur. Ceram. Soc.* **2009**, *29*, 1535.

[40] D. H. Ma, H. J. Wang, M. Niu, J. B. Wen, H. Wei, J. Zhou, J. P. Fan, D. H. Zhang, *Ceram. Int.* **2018**, *44*, 1443.

[41] C. Zhou, X. Gao, Y. Xu, G. Buntkowsky, Y. Ikuhara, R. Riedel, E. Ionescu, *J. Eur. Ceram. Soc.* **2015**, *35*, 2007.

[42] X. Zhang, Y. Duan, X. Dai, T. Li, Y. Xia, P. Zheng, H. Li, Y. Jiang, *Appl. Surf. Sci.* **2020**, *504*, 144437.

[43] A. Szekeres, P. Danesh, *J. Non-Cryst. Solids* **1995**, *187*, 45.

[44] F. Xu, B. Wagner, P. Ghildiyal, L. Mangolini, M. R. Zachariah, *Phys. Rev. Mater.* **2023**, *7*, 045403.

[45] J. B. Wen, S. Huang, H. J. Wang, *Key Eng. Mater.* **2014**, *602–603*, 367.

[46] B. Liang, Z. Yang, Y. Li, J. Yuan, D. Jia, Y. Zhou, *Ceram. Int.* **2015**, *41*, 8868.

[47] D. Li, Z. Yang, D. Jia, X. Duan, P. He, Y. Zhou, *Corros. Sci.* **2015**, *100*, 85.

[48] X. Long, Z. Wu, C. Shao, X. Wang, Y. Wang, *J. Adv. Ceram.* **2021**, *10*, 768.

**2400677 (9 of 9)**